Supporting Information

Conformable Nanowire-in-Nanofiber Hybrids for Low-Threshold Optical Gain in the Ultraviolet

Alberto Portone[†,‡,§], Rocio Borrego-Varillas[#], Lucia Ganzer[#], Riccardo Di Corato[⊥], Antonio Qualtieri[∥], Luana Persano[†,‡], Andrea Camposeo[†,‡], Giulio Cerullo[#,] and Dario Pisignano[†,¶,*]*

[†]NEST, Istituto Nanoscienze-CNR, Piazza S. Silvestro 12, I-56127 Pisa, Italy

[‡]NEST, Scuola Normale Superiore, Piazza S. Silvestro 12, I-56127 Pisa, Italy

[§]Dipartimento di Matematica e Fisica "Ennio De Giorgi", Università del Salento, Via Arnesano I-73100, Lecce, Italy

[#]IFN-CNR, Dipartimento di Fisica, Politecnico di Milano, Piazza L. da Vinci 32, I-20133 Milano, Italy

[⊥]Institute for Microelectronics and Microsystems, CNR-IMM, Campus Ecotekne, Via Monteroni, I-73100 Lecce, Italy.

[∥]Center for Biomolecular Nanotechnologies, Istituto Italiano di Tecnologia, Via Barsanti, I-73010 Arnesano (LE), Italy.

[¶]Dipartimento di Fisica, Università di Pisa, Largo B. Pontecorvo 3, I-56127 Pisa, Italy.

*Corresponding authors, giulio.cerullo@polimi.it, dario.pisignano@unipi.it

Keywords: organic-inorganic materials, nanocomposites, zinc oxide, electrospinning, amplified spontaneous emission, ultrafast transient absorption

1. Solubility Tests

To identify a good solvent, able to disperse the nanomaterials and to avoid aggregation and precipitation during the solution preparation and the electrospinning process, extensive solubility tests have been performed by mixing ZnO nanoparticles (NPs) with common solvents and mixtures of them. To this aim, 50 mg mL^{-1} of NPs have been dispersed in (1) acetone, (2) chloroform, (3) a mixture of chloroform and dimethylformamide (ratio 1:1 volume/volume - v/v), (4) ethanol, (5) methanol, (6) a mixture of chloroform and ethanol (ratio 1:1 v/v). The NPs have been dispersed by an ultrasonic bath for 1 hour, and the resulting dispersions stored for 24 hours. As shown in Figure S1, after one day the NP-suspension in ethanol, methanol and in the mix of ethanol and chloroform is stable. On the contrary, NPs precipitate in absence of alcohols, forming a sediment.

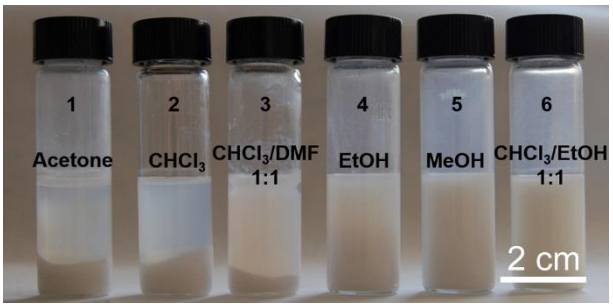

Figure S1. Photograph of ZnO NPs dispersed in various solvents: acetone (1), chloroform (2), chloroform and dimethylformamide with 1:1 (v/v) ratio (3), ethanol (4), methanol (5), chloroform and ethanol with 1:1 (v/v) ratio (6). Particle concentration: 50 mg mL^{-1}. Photograph acquired after 24 hs following dispersion by sonication. The suspensions in ethanol, methanol and in the mix of ethanol and chloroform are stable. On the contrary, NPs precipitate in absence of alcohols and form sediment. The chloroform/ethanol mixture is chosen for electrospinning experiments due to the very good solubility of PMMA in chloroform.

2. Size distribution

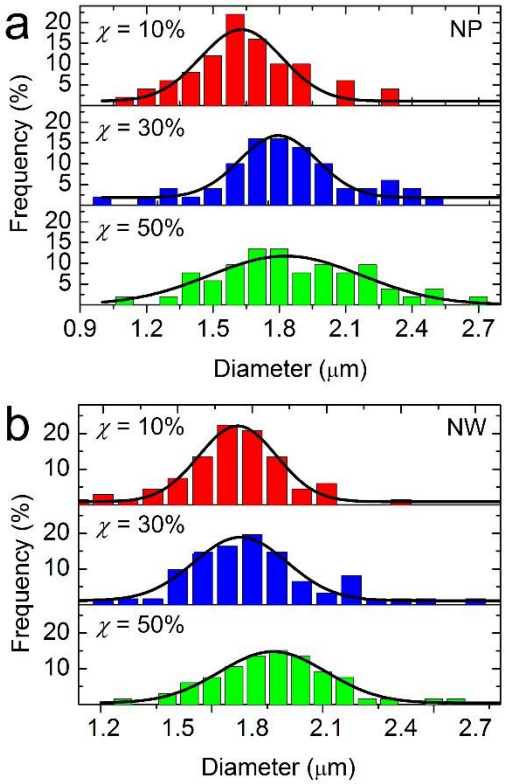

Figure S2. (a,b) Diameter distribution of fibers doped with ZnO NPs (a) and ZnO NWs (b), electrospun from solutions at various ZnO/polymer relative weight ratio (χ = 10%, 30%, and 50%). The superimposed black lines are Gaussian fits to experimental data.

3. TEM analysis

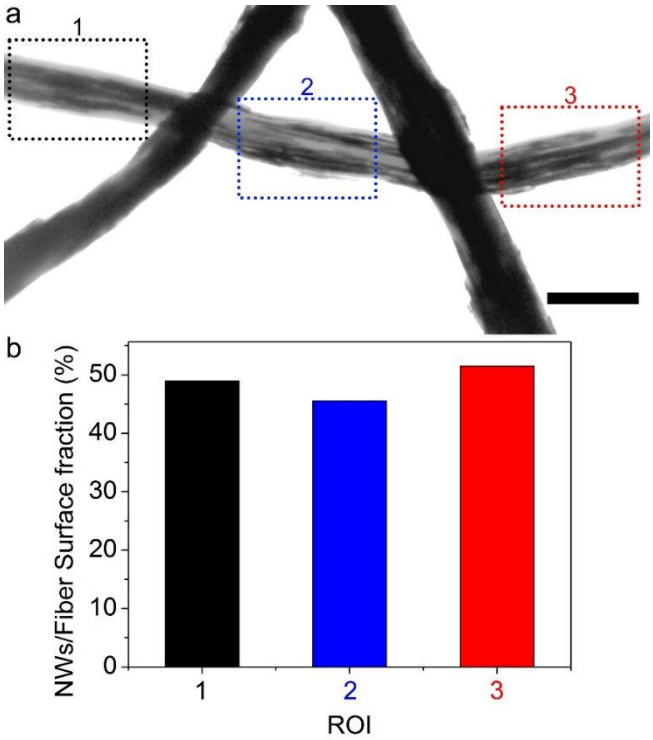

Figure S3. (a) TEM micrograph of fibers doped with ZnO NWs. χ = 30%. Scale bar: 2 μm. (b) Projected, shadowed area corresponding to NWs in the three regions of interest (ROIs) shown in (a).

TEM imaging was exploited to give an estimation of the ZnO/PMMA volumetric ratio in the hybrid fibers. An example of a TEM micrograph of a single hybrid fiber is shown in Figure S4. NWs are visible as darker areas with different signal intensities that can be attributed to two or more overlapping NWs along the path of the electron beam. Brightness and contrast of the image were set to highlight as much as possible the presence of NWs in the polymer matrix. The volume occupied by the NWs can be estimated by considering the area, A_1, of the darker regions as due to packed and uniaxially aligned NWs, with length 1 μm and diameter 40 nm. The ratio between A_1 and the cross-sectional area of a single NW ($A_{NW} \cong 2L_{NW} \times r_{NW}$, where L_{NW} and r_{NW} are the length and radius of the ZnO NW) gives the number of NWs in the area A_1 ($N_1 = A_1/A_{NW}$) and allows their total volume ($V_1 = N_1 \times V_{NW} = N_1 \times L_{NW} \times \pi r_{NW}^2$) to be calculated. The extension of A_1 is shown in Figure S4b, where a thresholding method was applied to the original image to remove the signal due to the polymer matrix. Briefly, in a grayscale image (whose scale, *s*, ranges from 0, that corresponds to black, to 255, that corresponds to white) the method set to white the intensity of those pixels whose *s* value is higher than a fixed value (threshold value) and to black the intensity of those pixels whose *s* is lower than the threshold value. The black area of Figure S4b was measured and considered as A_1. Such estimation can be improved by considering that in some areas there is an overlap of two NWs, as highlighted by the red arrow in Figure S4a. To account for this effect, the TEM micrograph was processed by selecting a different threshold value, *i.e*. a value lower than the one used for estimating A_1 and also lower than the *s* value for a single NW, as the one highlighted by the blue arrow in Figure S4. Indeed, the area highlighted by the blue arrow is black in Figure S4b, and it is included in the calculation of the area of A_1, while it is white after the second thresholding (Figure S4c). In this way, the extension of an area A_2 (black area in Figure S4c) can be utilized to estimate the number of NWs, N_2, whose shadowed

regions overlap with those included in the area A_1. This set of NWs occupies a volume V_2. This approach was iterated, by applying a filter that removes areas with intensity similar to regions with two overlapping NWs (Figure S4d) and obtaining a volume V_3 of NWs. The NW/PMMA volumetric ratio can be calculated as the ratio between the sum $V_1+V_2+V_3$ and the volume of the polymer fiber, obtaining a value of about 6%. This is in line with the expected one, calculated starting from the experimental weight ratio used for sample preparation. In fact, considering the ZnO mass density, D_{ZnO}=5.4 g cm^{-3} and the PMMA one, D_{PMMA}=1.19 g cm^{-3}, samples realized starting from a solution with χ = 30%, would feature a NW/PMMA volumetric ratio of 6.6%.

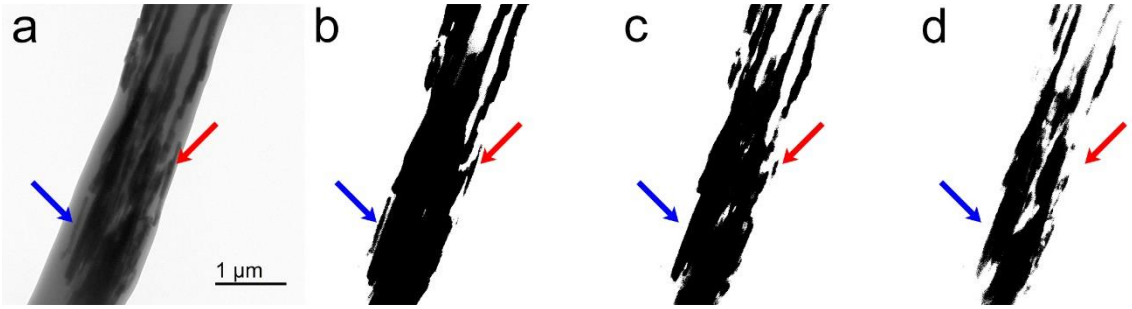

Figure S4. (a) TEM micrograph of a ZnO NW-in fiber hybrid (χ = 30%), used for the estimation of the volumetric ratio between NWs and PMMA matrix. (b-d) Micrographs converted into binary images by the application of a threshold which selects the regions (black areas) with grayscale intensity lower than 31% (b), 25.5% (c) and 19% (d) of the maximum intensity of the micrograph.

4. Optical properties

The effect of the fiber size and NW content on the light transport properties of the hybrids can be rationalized by considering a cylindrical waveguide with diameter, D, and refractive index, n_{eff}, and calculating the relative integrated intensities of the modes of electromagnetic field (with wavelength, λ = 382 nm, and wavenumber, $k = 2\pi/\lambda$) inside and outside the waveguide. This can be evaluated by calculating the fractional mode power, η, within the waveguide as follows:[1]

$$\eta = 1 - \frac{\left(2.405 exp\left[-\frac{2}{kD\sqrt{n_{eff}-1}}\right]\right)^2}{\left(0.5kD\sqrt{n_{eff}-1}\right)^3} \quad \text{(S1)}$$

Figure S5 shows the dependence of η on the waveguide diameter for a neat PMMA fiber ($n_{eff} = n_{PMMA} = 1.51$)[2] and for a fiber incorporating ZnO NWs (χ = 30%). For the hybrids, n_{eff} was estimated by utilizing the Maxwell Garnett expression for the refractive index of composite materials, which contain anisotropic particles as fillers with length (L_{NW}) much larger than their transversal size ($L_{NW} >> d_{NW}$).[3] The volumetric ratio between the ZnO NW fillers and the PMMA matrix was 6%, as estimated above. The resulting value of n_{eff} is 1.55. Figure S5 shows that for fibers with transversal size, D, larger than 1 μm, almost 99% of the field intensity is contained in the fiber, whereas a decrease of the fractional mode power occurs for D<250 nm, namely close to the cut-off size, $d_{cut\text{-}off}$. The value of $d_{cut\text{-}off}$ is about 160 nm for the hybrid fibers (and about 170 nm for pristine PMMA fibers), as estimated by the expression:[1] $d_{cut-off} \cong \frac{\lambda}{2\sqrt{n_{eff}^2-1}}$.

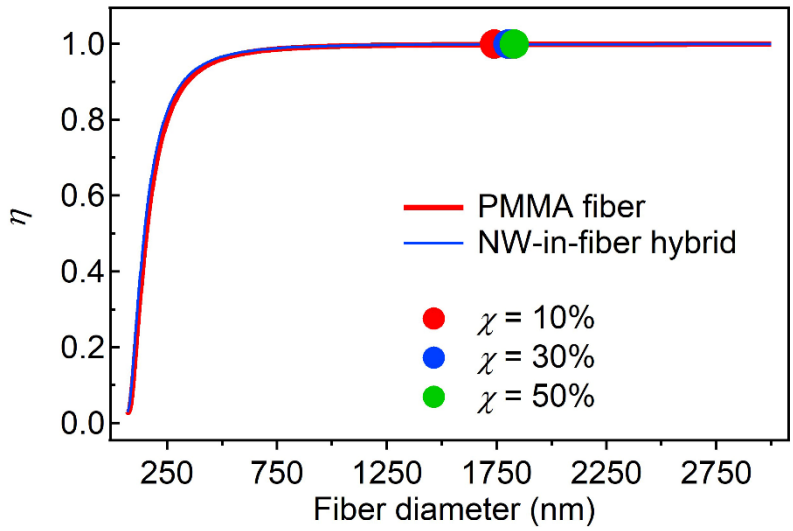

Figure S5. Calculated fractional mode power within a cylindrical waveguide, η, *vs*. the diameter of the fiber. The data are calculated for a neat PMMA fiber (red line, $n_{eff} = n_{PMMA} = 1.51$) and for a NW-in-fiber hybrid (blue line, $n_{eff} = 1.55$). The measured average diameter of the hybrid fibers obtained by electrospinning from solutions with χ = 10%, 30% and 50% ZnO NWs are marked by red, blue and green full circles, respectively.

The general behavior for light propagating in a complex waveguide constituted by a polymer matrix incorporating ZnO NWs can be captured taking into account the alignment of the NWs along the fiber longitudinal axis, as well as their elongated shape. Light can efficiently propagate in a fiber made of PMMA if the angle of incidence, β, at the fiber/air interface is larger than the critical angle ($\beta c = 41.5°$), as schematized in Figure S6a. Therefore, the light incident on a ZnO NW that is aligned along the fiber length will have local incidence angle, α_i, in the range ±48.5°. Such beams will be then diffused by the NW. If the direction of the scattered light will not meet the condition for internal total reflection, this light will be scattered out of the fiber, whereas it will be waveguided in case of diffusion angles in a range ±48.5° with respect to the fiber axis

(roughly parallel to NWs). To estimate the amount of light that fulfills this requirement, the angular dependence of the intensity of the light scattered by a NW is calculated under the Rayleigh-Gans approximation,[4] which is valid if $\left|\frac{n_{ZnO}}{n_{PMMA}} - 1\right|$ is well below unity and $\frac{\pi d_{NW}}{\lambda}\left|\frac{n_{ZnO}}{n_{PMMA}} - 1\right| \ll 1$, where d_{NW} is the diameter of the ZnO NWs (d_{NW}=40 nm) and n_{ZnO} is the refractive index of ZnO (n_{ZnO} = 2.45).[5] Under these conditions, the following expression can be used for the calculation of a form factor:[4]

$$f(\theta, \phi, \alpha_i) = \frac{8\sin\{0.5kL_{NW}[\cos\alpha_i - \sin\theta\cos(\phi)]\}}{kL_{NW}[\cos\alpha_i - \sin\theta\cos(\phi)]} \frac{J_1(0.5kd_{NW}\sqrt{\sin^2\theta\sin^2(\phi) + (\cos\theta - \sin\alpha_i)^2}}{kd_{NW}\sqrt{\sin^2\theta\sin^2(\phi) + (\cos\theta - \sin\alpha_i)^2}}$$

where L_{NW} is the ZnO NW length, while the angles θ, ϕ and α_i are introduced in Figure 6a. The intensity of the light scattered by the NW is proportional to the squared form factor[4] and, consequently, the calculation of $f^2(\theta, \phi)$ provides useful information about the angular distribution of intensity of light scattered by a NW embedded in PMMA. The results of such calculations for various angle of incidence are shown in Figure S6b-g, which evidences that most of the scattering occurs in the NW forward direction and in an angular range that allows for propagation along the fiber by total internal reflection.

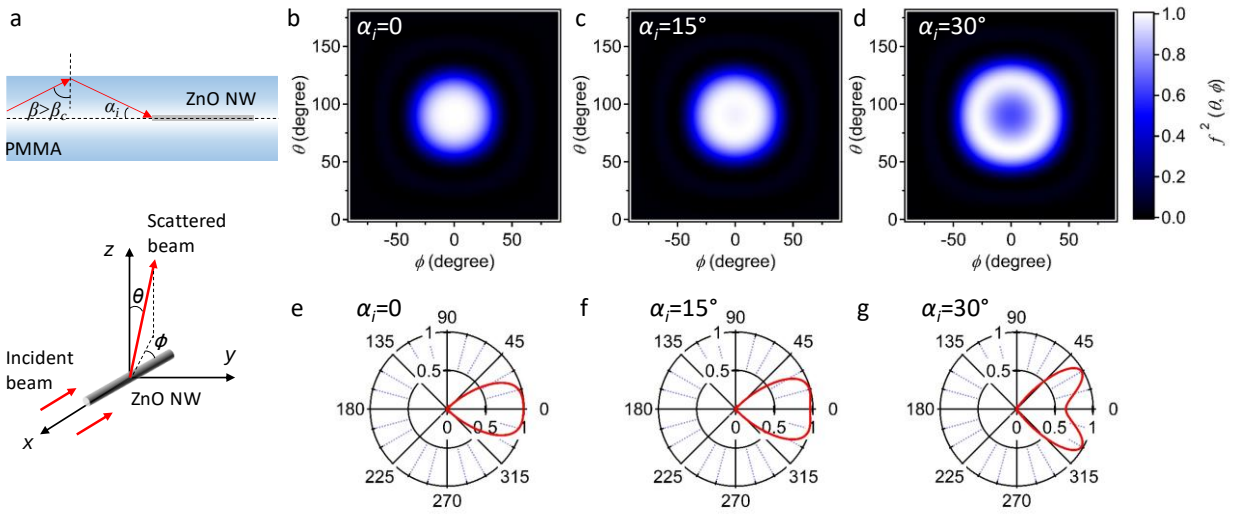

Figure S6. (a) Scheme of a light beam guided along a NW-in-fiber waveguide (top scheme) and of the light beam incident and scattered by an embedded ZnO NW (bottom scheme). (b-d) Dependence of the squared form factor, $f^2(\theta, \phi)$, on the scattering angles θ and ϕ, that are schematized in the bottom scheme of (a), for different angles of incidence (α_i) of the beam propagating in the fiber waveguide. (e-g) Corresponding dependence the squared form factor on ϕ in the *x*-*y* plane ($\theta = 0$). In (e)-(g) the incident beam propagates from left to right, whereas $\phi =$ 0 (180°) is the direction of forward(backward) scattering.

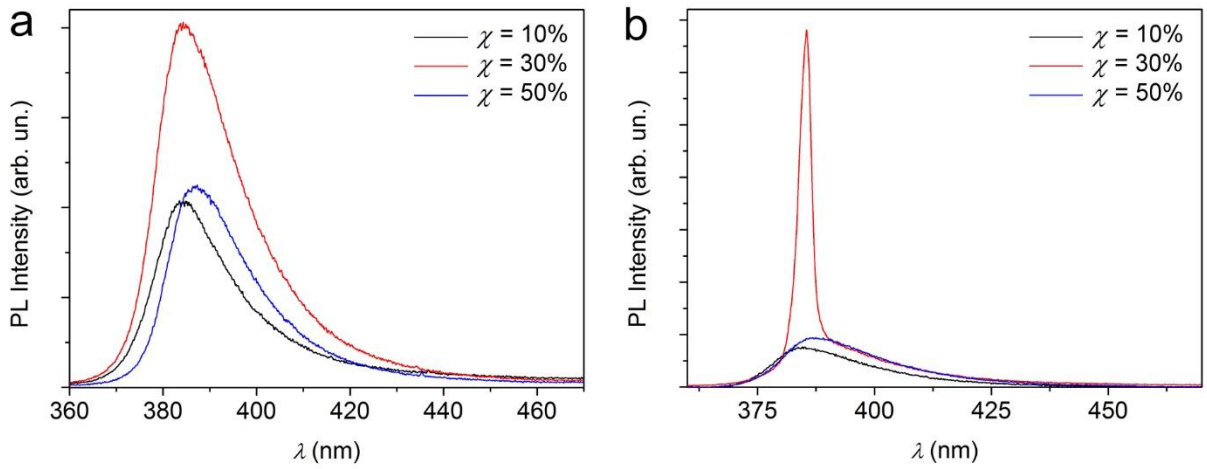

Figure S7. Comparison of PL emission (a) and ASE (b) in NW-in-fibers electrospun from solutions with χ = 10%, 30%, and 50%. Spectra are acquired with the same excitation and collection set-up. λ_{exc} = 355 nm. Excitation fluence: 0.2 mJ cm^{-2} (a) and 1.8 mJ cm^{-2} (b).

The photoexcited carrier density has been estimated by considering that the pump pulse has an energy, E_p = 20 nJ, and a beam diameter in the focus, d = 100 μm, corresponding to a fluence $F = E_p/(\pi d^2/4) \cong 250$ μJ/cm^2. Given the pump pulse photon energy of 3.7 eV (corresponding to 335 nm wavelength) we obtained an incident pump photon flux of 42.2×10^{13} photons/cm^2. Considering the optical density of the sample (OD = 0.2 at 3.7 eV), and the corresponding absorbance $A = 1\text{-}10^{-OD} = 0.37$, we obtained an absorbed photon flux of 15.6×10^{13} photons/cm^2. Finally, assuming a uniform carrier density across a sample thickness of 23 μm, which is a justified approximation given the comparatively low optical density, we finally estimated a photoexcited carrier density of 6.78×10^{16} carriers/cm^3.

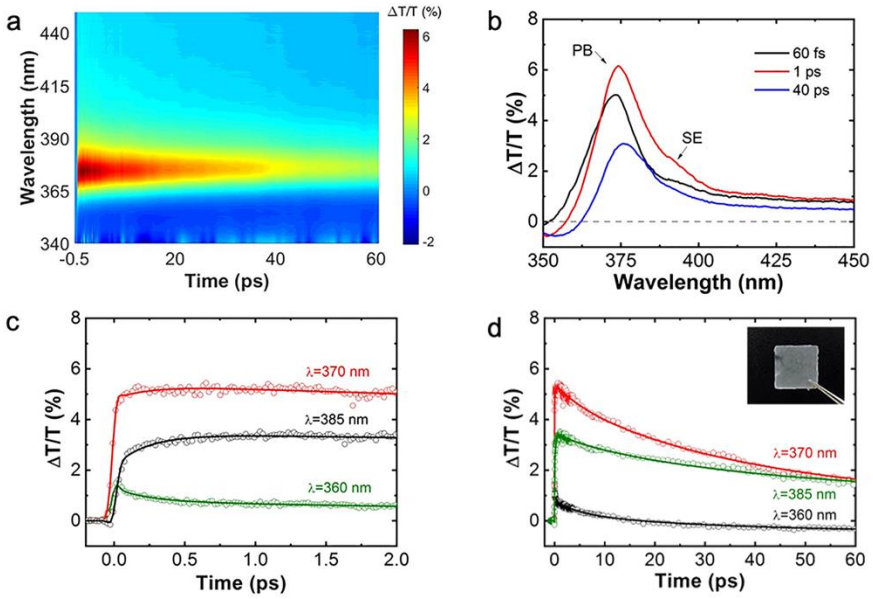

Figure S8. Femtosecond pump-probe spectroscopy of fibers with ZnO NPs. (a) 2D $\Delta T/T$ map as a function of probe wavelength and pump-probe delay. (b) $\Delta T/T$ spectra at selected pump-probe delays. (c,d) $\Delta T/T$ dynamics at selected probe wavelengths for short (c) and long (d) delays. Pump-probe measurements are performed on samples electrospun from solutions with χ = 10% - see picture in the inset of panel (d)-, analogously to Figure 5.

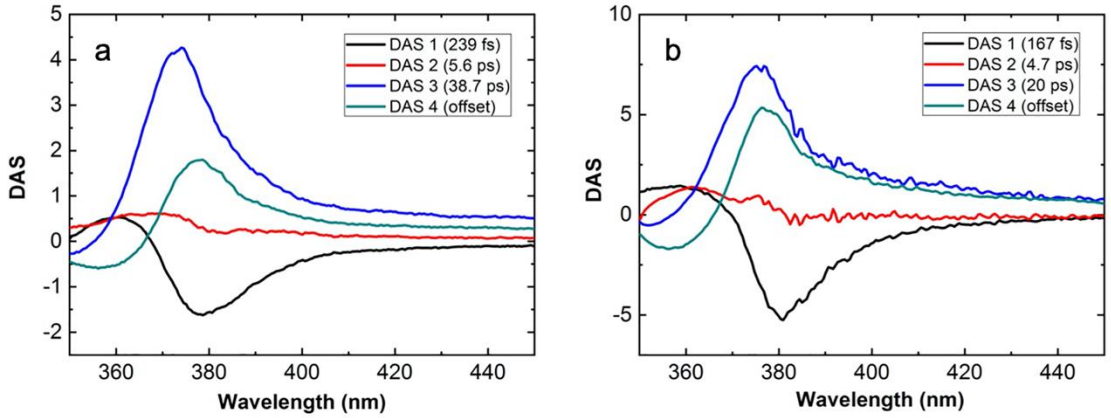

Figure S9. Decay associated spectra (DAS) for the femtosecond pump-probe measurements on the fibers with ZnO NWs (a) and NPs (b).

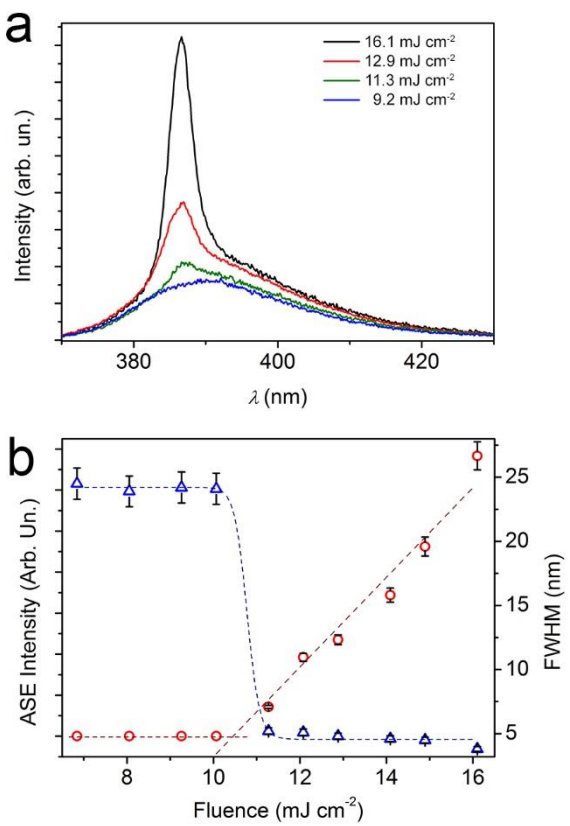

Figure S10. (a) ASE spectra of NW-doped films for different pumping fluences. (b) ASE intensity (red circles, left vertical scale) and full width at half maximum (FWHM) of the spectra (blue triangles, right vertical scale) as a function of the pumping fluence.

UV emitter	ASE/ Laser	Max. emission wavelength (nm)	Threshold (mJ cm^{-2})	Threshold (kW cm^{-2})	FWHM (nm)	Polarization	Divergence (mrad)	Flexible/ Conformable	Ref.
ZnO NWs-in-fiber hybrids	ASE	382	0.6	60	4	Polarized	5	Yes	This work
Polymer fibers doped with organic dye	ASE	387	0.1	10	11	-	16.5	Yes	6
ZnO NPs - polymer film	Laser	387	2.8	-	4	-	-	Yes	7
Organic semicon-ductor film	ASE	394	1.3×10^{-3}	2.6	3.6	-	-	-	8
ZnO NWs array	Laser	385	-	40	<0.3	-	-	-	9
ZnO NW	Laser	385	7×10^{-5}	-	0.25-1	Polarized	-	-	5
Hexagonal ZnO Microdisks	Laser	390	0.28	280	0.12	-	-	-	10
GaN NW	Laser	375	7×10^{-4}	-	<1	-	-	-	11
GaN NW /silica layer/Al film	Laser	370	-	3500	0.8	Polarized	-	-	12
2,4,5-triphenyl-imidazole NW	Laser	375	-	-	<4	-	-	-	13

Table S1. Comparison of the emission properties of ZnO NW-in-fiber hybrids (this work) and other UV-emitting materials which show amplified emission and lasing under optical pumping.

References

1 O'Carroll, D.; Lieberwirth, I.; Redmond, G., Microcavity Effects and Optically Pumped Lasing in Single Conjugated Polymer Nanowires. *Nat. Nanotechnol.* **2007**, *2*, 180-184.

2 Badie, G.; Brindza, M.; Flynn, R. A.; Rosenberg, A.; Shirk, J. S., Refractive Index Measurements of Poly(methyl methacrylate) (PMMA) from 0.4–1.6 μm. *Appl. Opt.* **2015**, *54*, F139-F143.

3 Markel, V. A., Introduction to the Maxwell Garnett Approximation: Tutorial. *J. Opt. Soc. Am. A* **2016**, *33*, 1244-1256.

4 Bohren, C. F.; Huffman, D. R. *Absorption and Scattering of Light by Small Particles*, 1st edition; Wiley-VCH Verlag: Weinheim, 2004; 158-165.

5 Johnson, J. C.; Yan, H.; Yang, P.; Saykally, R. J., Optical Cavity Effects in ZnO Nanowire Lasers and Waveguides. *J. Phys. Chem. B* **2003**, *107*, 8816-8828.

6 Morello, G.; Manco, R.; Moffa, M.; Persano, L.; Camposeo, A.; Pisignano, D., Multifunctional Polymer Nanofibers: UV Emission, Optical Gain, Anisotropic Wetting, and High Hydrophobicity for Next Flexible Excitation Sources. *ACS Appl. Mater. Interfaces* **2015**, *7*, 21907-21912.

7 Anglos, D.; Stassinopoulos, A.; Das, R. N.; Zacharakis, G.; Psyllaki, M.; Jakubiak, R.; Anastasiadis, S. H., Random Laser Action in Organic–Inorganic Nanocomposites. *J. Opt. Soc. Am. B* **2004**, *21*, 208-213.

8 Kawamura, Y.; Yamamoto, H.; Goushi, K.; Sasabe, H.; Adachi, C.; Yoshizaki, H., Ultraviolet Amplified Spontaneous Emission from Thin Films of 4,4′-Bis(9-carbazolyl)-2, 2′-Biphenyl and the Derivatives. *Appl. Phys. Lett.* **2004**, *84*, 2724-2726.

9 Huang, M. H.; Mao, S.; Feick, H.; Yan, H.; Wu, Y.; Kind, H.; Weber, E.; Russo, R.; Yang, P., Room-Temperature Ultraviolet Nanowire Nanolasers. *Science* **2001**, *292*, 1897-1899.

10 Chen, R.; Ling, B.; Sun, X. W.; Sun, H. D., Room Temperature Excitonic Whispering Gallery Mode Lasing from High-Quality Hexagonal ZnO Microdisks. *Adv. Mater.* **2011**, *23*, 2199-2204.

11 Johnson, J. C.; Choi, H. J.; Knutsen, K. P.; Schaller, R. D.; Yang, P.; Saykally, R. J., Single Gallium Nitride Nanowire Lasers. *Nat. Mater.* **2002**, *1*, 106-110.

12 Zhang, Q.; Li, G.; Liu, X.; Qian, F.; Li, Y.; Sum, T. C.; Lieber, C. M.; Xiong, Q. A., A Room Temperature Low-Threshold Ultraviolet Plasmonic Nanolaser. *Nat. Commun.* **2014**, *5*, 4953.

13 Zhao, Y. S.; Peng, A.; Fu, H.; Ma, Y.; Yao, J., Nanowire Waveguides and Ultraviolet Lasers Based on Small Organic Molecules. *Adv. Mater.* **2008**, *20*, 1661-1665.